Original Article

Differentiation of benign and malignant lesions in Bethesda III and IV thyroid nodules via dual-energy computed tomography quantitative parameters and morphologic features

Xiaofang Ren, Zuhua Song, Dan Zhang, Xiaojiao Li, Jie Huang, Qian Liu, Youjia Wen, Jiayan Zhang, Dan Zeng, Zhuoyue Tang

Department of Radiology, Chongqing General Hospital, Chongqing, China

Contributions: (I) Conception and design: X Ren, Z Song, D Zhang; (II) Administrative support: Z Tang; (III) Provision of study materials or patients: Q Liu, D Zeng, Y Wen; (IV) Collection and assembly of data: X Li, J Huang, J Zhang; (V) Data analysis and interpretation: X Ren, Z Song; (VI) Manuscript writing: All authors; (VII) Final approval of manuscript: All authors.

Correspondence to: Zhuoyue Tang, MD. Department of Radiology, Chongqing General Hospital, No. 118, Xingguang Avenue, Liangjiang New Area, Chongqing 401147, China. Email: zhuoyue_tang@cqmu.edu.cn.

Background: Thyroid nodules (TNs) cytologically defined as category Bethesda III and IV pose a major diagnostic challenge before surgery, demanding new methods to reduce unnecessary diagnostic thyroid lobectomies for patients with benign TNs. This study aimed to assess whether a model combining dual-energy computed tomography (DECT) quantitative parameters with morphologic features could reliably differentiate between benign and malignant lesions in Bethesda III and IV TNs.

Methods: Data from 77 patients scheduled for thyroid surgery for Bethesda III and IV TNs (malignant =48; benign =29) who underwent DECT scans were reviewed. DECT quantitative parameters including normalized iodine concentration (NIC), attenuation on the slope of spectral Hounsfield unit (HU) curve, and normalized effective atomic number (Zeff) were measured in the arterial phase (AP) and venous phase (VP). DECT quantitative parameters and morphologic features were compared between the malignant and benign cohorts. The receiver operating characteristic curve was performed to compare the performances of significant DECT quantitative parameters, morphologic features, or the models combining the DECT parameters, respectively, with morphologic features. A nomogram was constructed from the optimal performance model, and the performance was evaluated via the calibration curve and decision curve analysis.

Results: The areas under the receiver operating characteristic curve with 95% confidence interval (CI) of the NIC in the AP (AP-NIC), slope of spectral HU curve in the AP, and NZeff in the AP were 0.749 (95% CI: 0.641–0.857), 0.654 (95% CI: 0.530–0.778), and 0.722 (95% CI: 0.602–0.842), respectively. The model combining AP-NIC with enhanced blurring showed the highest diagnostic performance, with an area under the receiver operating characteristic curve (AUC), sensitivity, and specificity of 0.808, 0.854, and 0.655, respectively; it was then used to construct a nomogram. The calibration curve showed that the discrepancy between the prediction of the nomogram and actual observations was less than 5%. The decision curve analysis indicated the nomogram had a positive net benefit in threshold risk ranges of 14% to 58% or 60% to 91% for malignant Bethesda III and IV TNs.

Conclusions: The model combining AP-NIC with enhanced blurring could reliably differentiate between benign and malignant lesions in Bethesda III and IV TNs.

Keywords: Thyroid nodule (TN); cytology; dual-energy computed tomography (DECT); nomogram; diagnosis

Submitted Oct 26, 2023. Accepted for publication May 14, 2024. Published online Jun 14, 2024.
doi: 10.21037/qims-23-1511
View this article at: https://dx.doi.org/10.21037/qims-23-1511

Introduction

Thyroid nodules (TNs) are a common finding, detected in up to 65% of the general population (1). Accurate identification of the nature of TNs is crucial for both patients and clinicians, as it dictates the adoption of distinct management strategies. Ultrasound-guided fine-needle aspiration biopsy stands as the standard preoperative method for assessing TN status (2). Within the 2023 Bethesda System for reporting thyroid cytopathology, fine-needle aspiration biopsy results include atypia of undetermined significance (Bethesda III) and follicular neoplasm (Bethesda IV), which carry malignancy risks of 13–30% and 23–34%, respectively (3). These categories pose challenges in preoperative characterization, often leading to recommendations for diagnostic thyroid lobectomy. However, this invasive procedure inevitably results in unnecessary thyroid lobectomies for patients with benign Bethesda III and IV TNs, causing potential surgical complications and escalating healthcare expenditures (2,4,5). Consequently, there is a pressing need for novel methods to differentiate between benign and malignant lesions in Bethesda III and IV TNs.

Various imaging modalities, such as ultrasound and positron emission tomography, have been employed to discern the nature of Bethesda category III and IV TNs (6,7). Although ultrasound is the preferred method due to its cost-effectiveness and accessibility, its limitations lie in the overlapping of benign and malignant TN ultrasound features and its inability to depict the stereoscopic anatomy around the thyroid (4,8-10). Positron emission tomography, while capable of identifying malignant lesions in Bethesda III and IV TNs based on differential metabolism, is subject to inadequate management of some Bethesda IV TNs and poor specificity (39.8–50%), possibly due to neglecting the morphologic features of TNs (11-13). Thus, achieving accurate preoperative identification of malignant lesions in Bethesda III and IV TNs remains a considerable challenge.

Dual-energy application, an advanced functional imaging technique, offers quantitative information related to hemodynamics and specific components. It enables an objective identification of lesions and provides detailed stereoscopic anatomical information for comprehensive lesion assessment (14,15). Previous studies have confirmed the clinical applicability of dual-energy computed tomography (DECT) parameters in the diagnosis of thyroid diseases (16), detection of extrathyroidal extension (17), and assessment of lymphatic node metastasis in thyroid cancer (18). However, to the best of our knowledge, there is limited research on the value of DECT quantitative parameters and morphologic features specifically for discriminating between benign and malignant lesions in Bethesda III and IV TNs.

This study thus aimed to identify useful DECT quantitative parameters and morphologic features for distinguishing between benign and malignant lesions in Bethesda III and IV TNs. Additionally, we aimed to integrate these findings into a nomogram to facilitate clinical personalized assessment. We present this article in accordance with the TRIPOD reporting checklist (available at https://qims.amegroups.com/article/view/10.21037/qims-23-1511/rc).

Methods

Patients

This retrospective study was conducted in accordance with the Declaration of Helsinki (as revised in 2013) and was approved by the Review Committee of Chongqing General Hospital (No. KY S2023-061-01). The requirement of informed consent from participants in this retrospective study was waived. The selected data in this study were derived from patients who received cytological diagnosis after ultrasound-guided fine-needle aspiration biopsy and who underwent DECT scans between August 2021 to June 2023. The inclusion criteria were the following: (I) a cytological diagnosis of Bethesda III or IV and (II) surgical pathological results available within 2 weeks after the DECT scan. Meanwhile, the exclusion criteria were as follows: (I) unqualified DECT image; (II) nodules with extensive calcification, cystic change, or necrosis; (III) patients with diffuse thyroid disease (involvement of the entire thyroid gland) (19); and (IV) nodule diameter <5 mm. Ultimately, 77 patients were enrolled. The patient eligibility flowchart is shown in *Figure 1*.

DECT acquisition technique

All patients underwent preoperative noncontrast and neck contrast-enhanced computed tomography (CT) scans with 64-slice DECT devices (IQon Spectral CT, Philips Healthcare, Amsterdam, the Netherlands). The DECT scanning protocol was as follows: tube voltage, 120 kVp; tube current, modulated with automated exposure control (DoseRight system, Philips Healthcare); detector

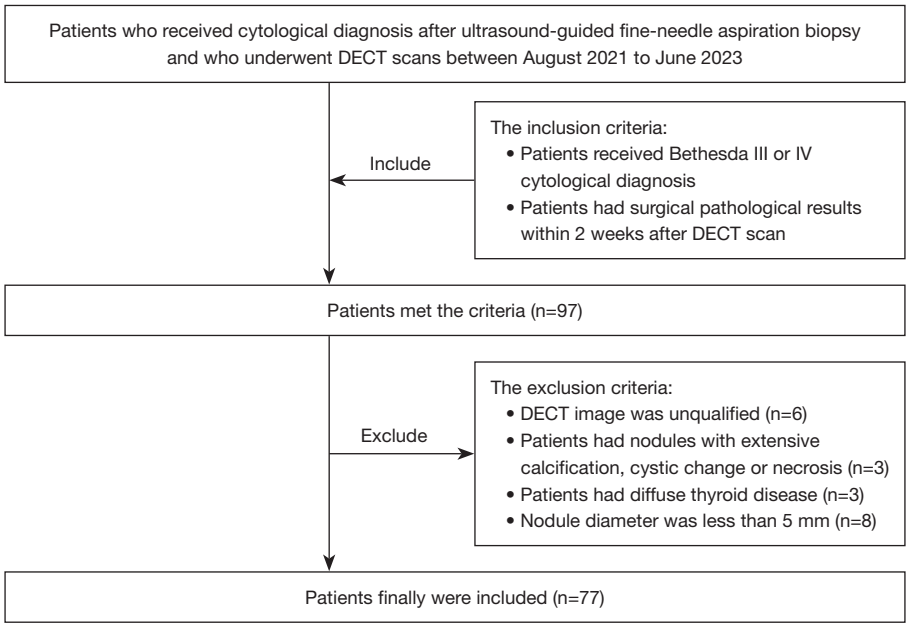

Figure 1 Flowchart of patient selection. DECT, dual-energy computed tomography.

collimation, 64×0.625 mm; field of view, 350 mm; matrix, 512×512; and reconstruction thickness, 0.67 mm. The noncontrast scan was performed first, and the contrast-enhance scan was conducted following injection of nonionic contrast media (iopamidol 350 mg/mL; Bracco, Milan, Italy) at a dose of 1.5 mL/kg and a rate of 3.5 mL/s, which was followed by a 30-mL saline flush at the same rate. The arterial phase (AP) scan was started with a threshold of 150 Hounsfield units (HU) in the descending aorta lumen at the tracheal bifurcation level, and the venous phase (VP) scan was started 40 seconds after the end of the AP scan.

DECT quantitative analysis

Two trained radiologists were blinded to the pathologic results and reconstructed DECT images at a spectral CT postprocessing workstation (IntelliSpace Portal version 10.1, Philips Healthcare) for the quantitative assessment of TNs. The generated DECT images included iodine images, 40- and 100-keV monochromatic images, and effective atomic number (Zeff) images in the AP and VP.

In conducting the quantitative analysis, we properly zoomed in on images to accurately assess lesions on the premise of ensuring a clear image. Second, a circular two-dimensional region-of-interest of the TN was manually drawn as large as possible, with calcification and cystic or necrotic regions being avoided, to acquire the following imaging parameters: HU on 40 and 100 keV monochromatic imaging, iodine concentration (IC), and Zeff. Another two-dimensional region of interest was then placed on the ipsilateral adjacent artery for subsequent normalized measurements to minimize the variations caused by the patient's circulation status. All DECT quantitative parameters were measured twice to calculate the average. Finally, the DECT quantitative parameters examined in the study included slope of the spectral HU curve (λHU), normalized iodine concentration (NIC), and normalized effective atomic number (NZeff) in the AP and VP. The formulae for these parameters were as follows: $\lambda HU = (HU_{40\ keV} - HU_{100\ keV})/(100 - 40)$; $NIC = IC_{nodule}/IC_{ipsilateral\ carotid\ artery}$; $NZeff = Zeff_{nodule}/Zeff_{ipsilateral\ carotid\ artery}$.

Morphological analysis

Morphological analysis of TNs was performed on the noncontrast, AP and VP images by two radiologists specializing in head-and-neck imaging who only knew the location of the lesion and who were blinded to the pathologic results of the TNs. Any disagreements were resolved via discussion. The DECT morphologic features included punctate calcification, irregular shape, enhanced blurring, and thyroid marginal interruption.

Table 1 Characteristics of patients and histopathological information

Characteristic	Patients (n=77)
Age* (years)	46.10±11.43
Sex	
Male	14
Female	63
Bethesda classification	
III	67
IV	10
Histopathological type	
Benign nodules	29
Fibrotic nodule	1
Nodular goiter	20
Follicular adenoma	3
Hashimoto thyroiditis	4
Granulomatous thyroiditis	1
Malignant nodules	48
Papillary carcinoma	14
Medullary carcinoma	1
Papillary microcarcinoma	33

Unless otherwise indicated, data are the number of patients. *, data are the mean ± standard deviation.

Punctate calcification was defined as the largest diameter of calcification ≤2 mm. Irregular shape was defined as neither a circular nor ovoid shape. Enhanced blurring was defined as the rim of the TN being more blurred on contrast enhancement image than on plain image and the density difference between the TN and surrounding thyroid parenchyma being decreased after enhancement CT scan. Thyroid marginal interruption was defined as a defect in the thyroid capsule.

Statistical analysis

Statistical analyses were performed using R software (The R Foundation for Statistical Computing; http://www.R-project.org), SPSS version 25.0 (IBM Corp., Armonk, NY, USA), MedCalc version 18.2.1 (MedCalc Software, Ostend, Belgium), and Python version 3.10.9 (Python Software Foundation. Wilmington, DE, USA). The intraclass correlation coefficient was used to assess the interobserver agreement for the DECT quantitative parameters. A two-sided P value <0.05 was considered statistically significant.

The Shapiro-Wilk test was used to determine the data distribution. Continuous data are expressed as mean ± standard deviation if they fit a normal distribution or as median with the interquartile range if they did not. Categorical variables are expressed as numbers of lesions with percentages. Differences in DECT quantitative parameters and morphologic features between benign and malignant Bethesda III and IV TNs were compared with the two-sample *t*-test, the Mann-Whitney, or chi-square test as appropriate. Receiver operating characteristic curve analysis was applied to evaluate the diagnostic ability of the DECT quantitative parameters, morphologic features, and combined models integrating DECT parameters, respectively, with morphologic features via multivariable binary logistic regression analysis. The area under the receiver operating characteristic curve (AUC) with a 95% confidence interval (95% CI) was acquired to evaluate the diagnostic capability. The DeLong test was used for the comparisons between the AUCs. The cutoff value was determined by the maximum Youden index, and the sensitivity and specificity were calculated. A nomogram was then constructed for optimal diagnostic performance. Calibration curve and decision curve analysis were employed to assess nomogram goodness of fit and clinical utility, respectively. The random forest variable importance and Shapley additive explanations (SHAP) summary plots were applied to visualize each variable's contribution to the predictive performance.

Results

Patient demographic and pathologic characteristics

A total of 77 Bethesda III and IV TNs in 77 patients were included and then divided into two cohorts according to the histopathologic results: benign nodules (n=29) and malignant nodules (n=48). Among these patients, 14 were men (mean age ± standard deviation 41.79±10.11 years) within an age range of 28–65 years, while 63 were women (mean age ± standard deviation 47.06±11.55 years) aged of 22–67 years. The patient demographic and histopathologic information is summarized in *Table 1*.

Table 2 Univariate analysis of the benign and malignant nodule cohorts

Variable	Benign nodule cohort (n=29)	Malignant nodule cohort (n=48)	F value /Z value/χ^2 value	P value
CT morphologic features[#]				
Punctate calcification	6 (20.7)	7 (14.6)	0.480	0.49
Irregular shape	13 (44.8)	18 (37.5)	0.404	0.53
Enhanced blurring	9 (31.0)	31 (64.6)	8.151	0.004
Thyroid marginal interruption	20 (69.0)	31 (64.6)	0.155	0.69
DECT parameters				
AP-NIC	0.37 (0.30, 0.46)	0.28 (0.23, 0.36)	–3.648	<0.001
AP-λHU	4.19 (3.29, 5.06)	3.58 (2.71, 4.30)	–2.250	0.02
AP-NZeff	0.83 (0.79, 0.85)	0.79 (0.76, 0.82)	–3.248	0.001
VP-NIC*	0.73±0.20	0.74±0.17	1.227	0.90
VP-λHU	3.48 (2.70, 4.31)	3.60 (2.86, 4.20)	–0.121	0.90
VP-NZeff*	0.95±0.42	0.95±0.03	0.980	0.97

Unless otherwise indicated, data are median with the interquartile range in parentheses. [#], data are numbers of lesions with percentages; *, data are the mean ± standard deviation. CT, computed tomography; DECT, dual-energy computed tomography; AP, arterial phase; VP, venous phase; NIC, normalized iodine concentration; λHU, slope of the spectral Hounsfield unit curve; NZeff, normalized effective atomic number.

Differences in the DECT quantitative parameters and morphologic features between the malignant and benign cohorts

The DECT quantitative parameters and morphologic features of the benign and malignant nodule cohorts are summarized in *Table 2*. The intraclass correlation coefficients for all quantitative DECT parameters exceeded 0.75. For DECT quantitative parameters, significant differences were noted for NIC in the AP (AP-NIC) (P<0.001), λHU in the AP (AP-λHU) (P=0.02), and NZeff in the AP (AP-NZeff) (P=0.001). However, no significant differences were observed for NIC in the VP (VP-NIC) (P=0.90), λHU in the VP (VP-λHU) (P=0.90), or NZeff in the VP (VP-NZeff) (P=0.97). Regarding morphologic features, enhanced blurring showed significant differences between the benign and malignant nodule cohorts (P=0.004), while there were no significant differences between the two cohorts in terms of punctate calcification (P=0.49), irregular shape (P=0.53), or thyroid marginal interruption (P=0.69).

Diagnostic performance of enhanced blurring or DECT quantitative parameters

The AUC, 95% CI of the AUC, sensitivity, and specificity of enhanced blurring and the DECT quantitative parameters are shown in *Table 3* and *Figure 2A*. Enhanced blurring had an AUC of 0.668. Among the DECT quantitative parameters in the AP, AP-NIC exhibited the highest diagnostic performance, with an AUC of 0.749.

Diagnostic performance of the models combining enhanced blurring and DECT parameters

After significant DECT parameters were respectively integrated with enhanced blurring, a combined model was developed using multivariate binary logistic regression. The receiver operating characteristic curves of these combined models are illustrated in *Figure 2B*. *Table 4* details the diagnostic performance of significant DECT quantitative parameters respectively in combination with enhanced

Table 3 The diagnostic performance of enhanced blurring and DECT parameters

DECT parameter	AUC (95% CI)	Sensitivity	Specificity	Cutoff value	P value
Enhanced blurring	0.668 (0.542–0.793)	0.646	0.690	–	0.01
AP-NIC	0.749 (0.641–0.857)	0.813	0.448	0.661	0.001
AP-λHU	0.654 (0.530–0.778)	0.917	0.207	0.590	0.04
AP-NZeff	0.722 (0.602–0.842)	0.917	0.414	0.576	0.006

DECT, dual-energy computed tomography; AUC, area under the receiver operating characteristic curve; CI, confidence interval; AP, arterial phase; NIC, normalized iodine concentration; λHU, slope of the spectral Hounsfield unit curve; NZeff, normalized effective atomic number.

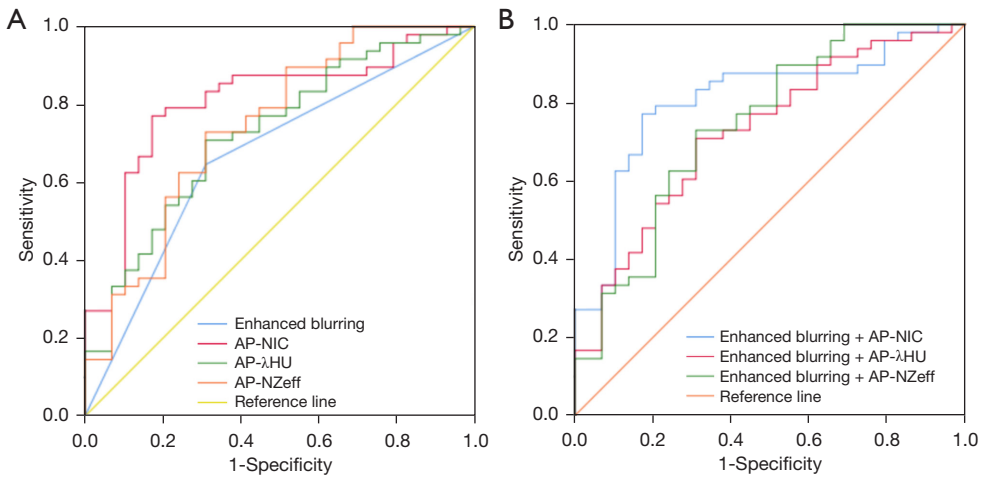

Figure 2 Receiver operating characteristic curves of DECT parameters. (A) Diagnostic performance of enhanced blurring and DECT quantitative parameters. (B) Diagnostic performance of the combined model with enhanced blurring and DECT parameters. AP, arterial phase; NIC, normalized iodine concentration; λHU, slope of the spectral Hounsfield unit curve; NZeff, normalized effective atomic number; DECT, dual-energy computed tomography.

Table 4 The diagnostic performance of the combined model with enhanced blurring and DECT parameters

DECT parameter	AUC (95% CI)	Sensitivity	Specificity	Cutoff value	P value
Enhanced blurring + AP-NIC	0.808 (0.707–0.910)	0.854	0.655	0.658	<0.001
Enhanced blurring + AP-λHU	0.724 (0.608–0.840)	0.792	0.483	0.568	0.001
Enhanced blurring + AP-NZeff	0.744 (0.627–0.860)	0.854	0.483	0.624	<0.001

DECT, dual-energy computed tomography; AUC, area under the receiver operating characteristic curve; CI, confidence interval; AP, arterial phase; NIC, normalized iodine concentration; λHU, slope of the spectral Hounsfield unit curve; NZeff, normalized effective atomic number.

blurring. The AUCs with 95% CIs of enhanced blurring + AP-NIC, enhanced blurring + AP-λHU, and enhanced blurring + AP-NZeff were 0.808 (95% CI: 0.707–0.910), 0.724 (95% CI: 0.608–0.840), and 0.744 (95% CI: 0.627–0.860), respectively. The P values of the DeLong test for the AUCs of different combinations are detailed in *Table 5*.

Performance of the nomogram and visualization of results using SHAP

The nomogram (*Figure 3*) was constructed based on the combined model with enhanced blurring and AP-NIC according to the following the formula: nomogram =

Table 5 P values of the DeLong test for AUC

DECT parameter	Enhanced blurring	AP-NIC	AP-λHU	AP-NZeff	Enhanced blurring + AP-NIC	Enhanced blurring + AP-λHU	Enhanced blurring + AP-NZeff
Enhanced blurring (AUC =0.668)	–	0.30	0.86	0.49	0.007	0.11	0.09
AP-NIC (AUC =0.749)	0.30	–	0.07	0.60	0.12	0.71	0.93
AP-λHU (AUC =0.654)	0.86	0.07	–	0.37	0.008	0.17	0.24
AP-NZeff (AUC =0.722)	0.49	0.60	0.37	–	0.14	0.98	0.63
Enhanced blurring + AP-NIC (AUC =0.808)	0.007	0.12	0.008	0.14	–	0.056	0.16
Enhanced blurring + AP-λHU (AUC =0.724)	0.11	0.71	0.17	0.98	0.056	–	0.69
Enhanced blurring + AP-NZeff (AUC =0.744)	0.09	0.93	0.24	0.63	0.16	0.69	–

AUC, area under the receiver operating characteristic curve; DECT, dual-energy computed tomography; AP, arterial phase; NIC, normalized iodine concentration; λHU, slope of the spectral Hounsfield unit curve; NZeff, normalized effective atomic number.

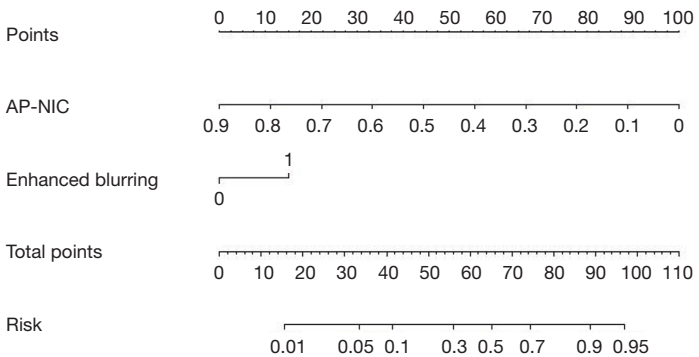

Figure 3 The nomogram based on the combination model for identifying malignant Bethesda III and IV thyroid nodules. The points of each predictor are obtained based on the "Points" bar. Subsequently, the sum of the two points is mapped to the "Total points" and "Risk" bars to thereby calculate the risk probability of malignant Bethesda III and IV thyroid nodules. AP, arterial phase; NIC, normalized iodine concentration.

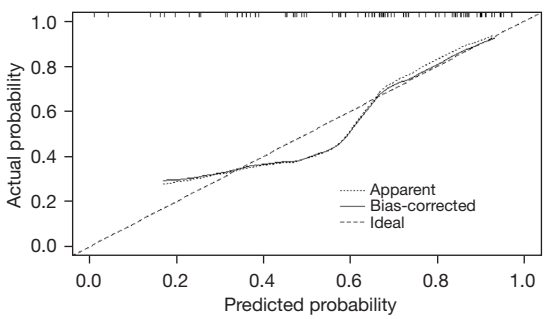

Figure 4 The calibration curves of the nomogram.

3.23 + 1.40 × enhanced blurring – 10.29 × AP-NIC. The calibration curve demonstrated a discrepancy of less than 5% between the nomogram's predictions and actual observations (*Figure 4*). The decision curve showed that the nomogram had positive a net benefit within threshold risk ranges of 14% to 58% or 60% to 91% for malignant Bethesda III and IV TNs (*Figure 5*). The variable importance plot (*Figure 6A*) and SHAP summary plot (*Figure 6B*) indicated that AP-NIC was the feature with the highest eigenvalues. An example of DECT and pathological imaging is shown in *Figure* 7.

Discussion

We found that the combined model integrating enhanced blurring with AP-NIC demonstrated superior performance compared to enhanced blurring alone. These findings indicated that the DECT quantitative parameters could serve as an effective complement to morphologic features for the preoperative diagnosis of malignant lesions in Bethesda III and IV TNs. Moreover, the nomogram based on the combined model was demonstrated to be an effective tool for the differential diagnosis of benign from malignant lesions in Bethesda III and IV TNs.

Our findings revealed that enhanced blurring exhibited the capacity to identify malignant lesions in Bethesda III and IV TNs, with an AUC of 0.668. We also found that enhanced blurring was more prevalent in malignant lesions than in benign ones, aligning partially with prior studies (20,21). This observation might be attributed to the increased neovascularization in the thyroid cancer's rim compared to its central area, resulting in density difference after enhancement and rendering thyroid cancer more similar to normal thyroid tissue (22,23). Surprisingly, no discernible differences were noted in punctate calcification, irregular shape, or thyroid marginal interruption, which is partially consistent with previous research (24,25). However, the disparate findings between several studies attempting to identify CT features of malignant TNs (26,27) may stem from variations in study cohorts, and notably, the subjectivity of the morphological assessments performed by observers. Additionally, only 64.6% of malignant TNs exhibited enhanced blurring in our study, emphasizing the need for a more accurate method for identifying malignancies in Bethesda III and IV TNs, especially those lacking typical morphologic features that tend to be easily overlooked by radiologists.

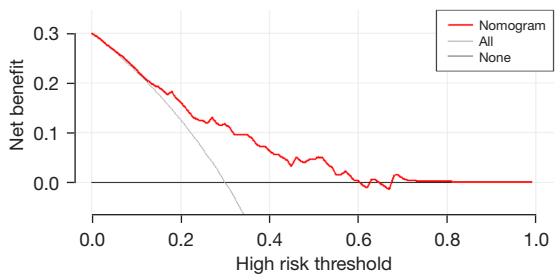

Figure 5 The decision curve analysis of the nomogram.

A previous paper proposed the utility of DECT quantitative parameters in objectively discerning malignant from benign lesions (28). Consistent with these findings, our study identified AP-NIC, AP-λHU, and AP-NZeff as valuable for preoperatively identifying malignant lesions in Bethesda III and IV TNs. AP-NIC, in particular, displayed the highest diagnostic performance among all the significant DECT parameters. The random forest variable importance and SHAP plots further supported the crucial role of AP-NIC as the most significant predictor of thyroid malignancy. The results indicated that the AP-NIC of malignant lesions was lower than that of benign lesions in Bethesda III and IV TNs. One possible explanation for this is that thyroid follicular cells with iodine uptake function are still present in benign TNs but not in thyroid cancers, leading to a lower IC of the malignant lesion (29,30). IC in tissues and that measured in DECT are highly similar (31). Hence, the NIC in our study, calculated based on the IC, was lower in

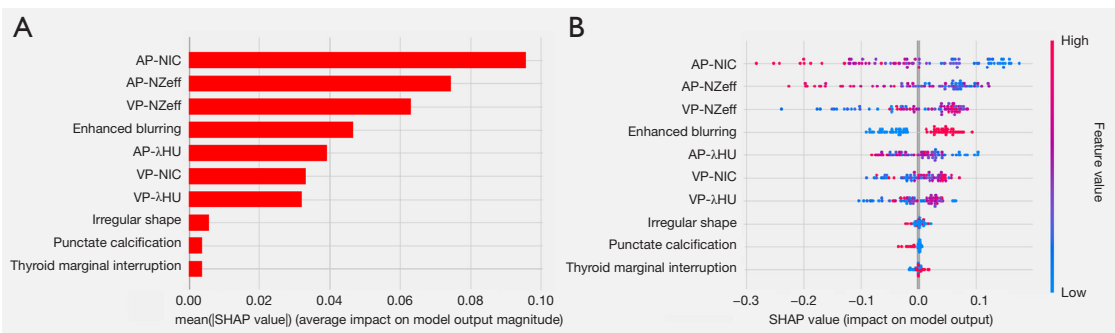

Figure 6 Feature importance visualization. (A) Feature importance plot. (B) SHAP summary plot. The abscissa indicates the SHAP value, and each line indicates a variable. The red dots represent higher feature values, while the blue dots denote lower feature values. AP, arterial phase; NIC, normalized iodine concentration; NZeff, normalized effective atomic number; VP, venous phase; λHU, slope of the spectral Hounsfield unit curve; SHAP, Shapley additive explanation.

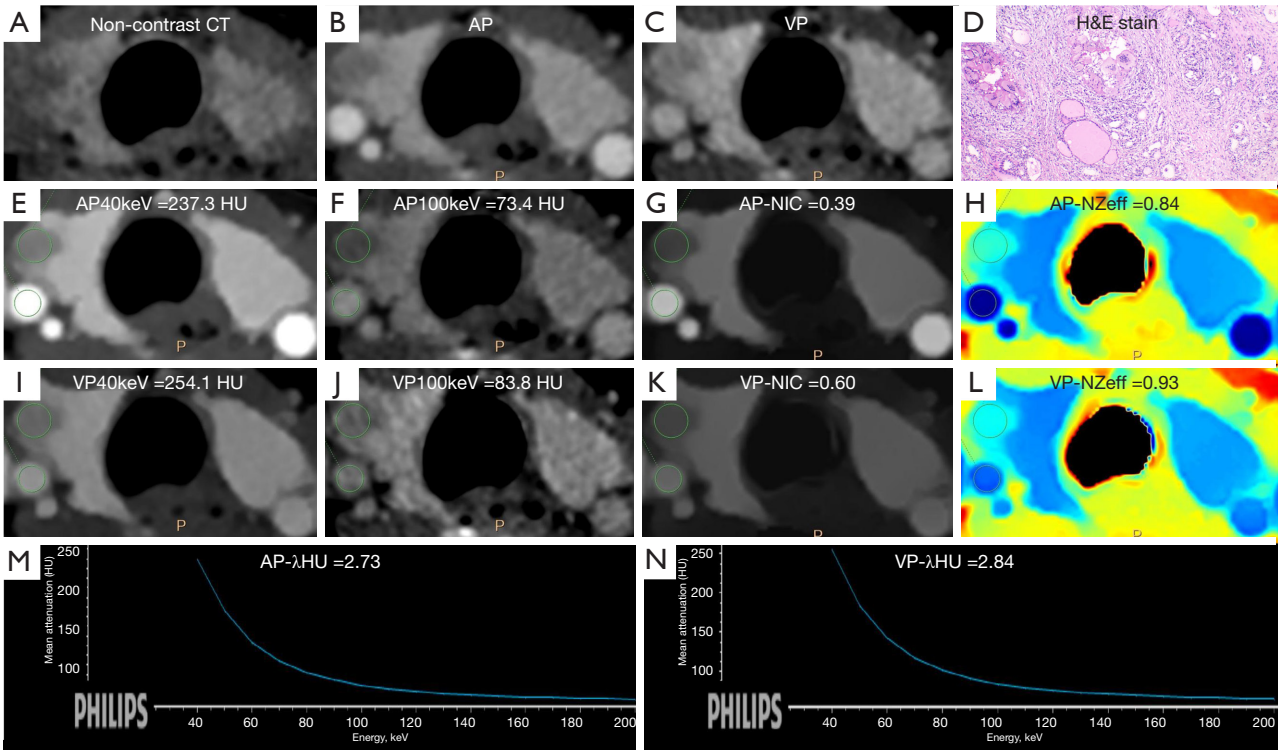

Figure 7 The DECT quantitative parameters and HE staining in a 32-year-old woman with granulomatous thyroiditis. In axial noncontrast and contrast-enhanced CT images, the rim of the thyroid nodule was more obscure after the enhanced CT scan (A-C). The HE-stained photomicrograph (original magnification, 40×) confirmed the nodule as granulomatous thyroiditis (D). The CT values on 40- and 100-keV monochromatic images in the AP were 237.3 and 73.4 HU, respectively (E,F). NIC, NZeff, and λHU in the AP were 0.39 (G), 0.84 (H), and 2.73 (M), respectively. The CT values on 40- and 100-keV monochromatic images in the VP were 254.1 and 83.8 HU, respectively (I,J). NIC, NZeff, and λHU in the VP were 0.60 (K), 0.93 (L), and 2.84 (N), respectively. The green circles represent the regions of interest. CT, computed tomography; AP, arterial phase; P, posterior; VP, venous phase; HE, hematoxylin and eosin; HU, Hounsfield unit; NIC, normalized iodine concentration; NZeff, normalized effective atomic number; λHU, slope of the spectral Hounsfield unit curve; DECT, dual-energy computed tomography.

malignant lesions than in benign lesions in Bethesda III and IV TNs. Furthermore, our findings revealed no significant differences in any of the quantitative DECT parameters assessed during the VP. This might be attributable to the intricately arranged and tortuous microvessels in malignant lesions that result in slow contrast flows. Additionally, cancer embolus in microvessels could contribute to this process. Iodinated contrast leaking into the intercellular space through loosely connected capillary endothelial cells in malignant lesions may also facilitate a slow iodinated contrast discharge in the VP, concealing the differences in DECT morphologic features parameters between benign and malignant Bethesda III and IV TNs (32). Chen *et al.* similarly reported that the diagnostic performance of DECT quantitative parameters in the AP outperformed those in the VP in predicting central lymph node metastases in patients with papillary thyroid cancer (33).

The addition of DECT parameters to enhanced blurring yielded satisfactory results for identifying malignant lesions in Bethesda III and IV TNs. The combined model that incorporated enhanced blurring and AP-NIC demonstrated the highest diagnostic utility in distinguishing benign from malignant lesions in Bethesda III and IV TNs, achieving an AUC, sensitivity, and specificity of 0.808, 0.854, and 0.655, respectively. Nomograms, as a simple visual representation of statistics-based tools, hold promise for evaluating the numerical probability of a clinical occurrence and aiding in the personalized management of patients (34). Decision curve analysis showed that the nomogram based on the combination model exhibited good clinical utility for

patients with Bethesda III and IV TNs. Therefore, this nomogram may serve as a straightforward, objective, and reliable tool for assisting in individualized assessment in clinic.

This study has certain limitations which should be acknowledged. First, we employed a single-center, retrospective design with a relatively small sample size, especially for the Bethesda IV TNs. Further studies with a larger sample size are required to confirm our findings. Second, all patients enrolled in this study underwent thyroid surgery, which might have introduced selection bias. Third, papillary carcinomas and nodular goiters were predominant among malignant nodules and benign nodules, respectively. Consequently, the study's findings may not be applicable to the detection of other pathological varieties of TNs.

Conclusions

Our findings suggest that AP-NIC has potential as an imaging biomarker for characterizing Bethesda III and IV TNs. The constructed nomogram that incorporates enhanced blurring and AP-NIC may serve as a convenient tool for accurately and reliably differentiating between benign and malignant lesions in Bethesda III and IV TNs, which may help decrease the need for diagnostic thyroid lobectomy.

Acknowledgments

The authors would like to thank all the volunteers who participated in the study and the staff of the Department of Radiology, Chongqing General Hospital, China, for their selfless and valuable assistance.

Funding: This study was funded by the Medical Research Key Program of the Combination of the Chongqing National Health Commission and Chongqing Science and Technology Bureau (No. 2019ZDXM010), the Medical Research Program of the Combination of Chongqing National Health Commission and Chongqing Science and Technology Bureau (No. 2020FYYX151), and the Chongqing Postdoctoral Science Foundation (No. CSTB2022NSCQ-BHX0737).

Footnote

Reporting Checklist: The authors have completed the TRIPOD reporting checklist. Available at https://qims.amegroups.com/article/view/10.21037/qims-23-1511/rc

Conflicts of Interest: All authors have completed the ICMJE uniform disclosure form (available at https://qims.amegroups.com/article/view/10.21037/qims-23-1511/coif). The authors have no conflicts of interest to declare.

Ethical Statement: The authors are accountable for all aspects of the work in ensuring that questions related to the accuracy or integrity of any part of the work are appropriately investigated and resolved. This study was conducted in accordance with the Declaration of Helsinki (as revised in 2013) and was approved by the Review Committee of Chongqing General Hospital (No. KY S2023-061-01). The requirement for informed consent from participants in this retrospective study was waived.

References

1. Durante C, Grani G, Lamartina L, Filetti S, Mandel SJ, Cooper DS. The Diagnosis and Management of Thyroid Nodules: A Review. JAMA 2018;319:914-24.
2. Haugen BR, Alexander EK, Bible KC, Doherty GM, Mandel SJ, Nikiforov YE, Pacini F, Randolph GW, Sawka AM, Schlumberger M, Schuff KG, Sherman SI, Sosa JA, Steward DL, Tuttle RM, Wartofsky L. 2015 American Thyroid Association Management Guidelines for Adult Patients with Thyroid Nodules and Differentiated Thyroid Cancer: The American Thyroid Association Guidelines Task Force on Thyroid Nodules and Differentiated Thyroid Cancer. Thyroid 2016;26:1-133.
3. Ali SZ, Baloch ZW, Cochand-Priollet B, Schmitt FC, Vielh P, VanderLaan PA. The 2023 Bethesda System for Reporting Thyroid Cytopathology. Thyroid 2023;33:1039-44.
4. Patel KN, Yip L, Lubitz CC, Grubbs EG, Miller BS, Shen W, Angelos P, Chen H, Doherty GM, Fahey TJ 3rd, Kebebew E, Livolsi VA, Perrier ND, Sipos JA, Sosa JA, Steward D, Tufano RP, McHenry CR, Carty SE. The American Association of Endocrine Surgeons Guidelines

for the Definitive Surgical Management of Thyroid Disease in Adults. Ann Surg 2020;271:e21-93.
5. Rosato L, Avenia N, Bernante P, De Palma M, Gulino G, Nasi PG, Pelizzo MR, Pezzullo L. Complications of thyroid surgery: analysis of a multicentric study on 14,934 patients operated on in Italy over 5 years. World J Surg 2004;28:271-6.
6. Celletti I, Fresilli D, De Vito C, Bononi M, Cardaccio S, Cozzolino A, Durante C, Grani G, Grimaldi G, Isidori AM, Catalano C, Cantisani V. TIRADS, SRE and SWE in INDETERMINATE thyroid nodule characterization: Which has better diagnostic performance? Radiol Med 2021;126:1189-200.
7. Piccardo A, Puntoni M, Treglia G, Foppiani L, Bertagna F, Paparo F, Massollo M, Dib B, Paone G, Arlandini A, Catrambone U, Casazza S, Pastorino A, Cabria M, Giovanella L. Thyroid nodules with indeterminate cytology: prospective comparison between 18F-FDG-PET/CT, multiparametric neck ultrasonography, 99mTc-MIBI scintigraphy and histology. Eur J Endocrinol 2016;174:693-703.
8. Nemec U, Nemec SF, Novotny C, Weber M, Czerny C, Krestan CR. Quantitative evaluation of contrast-enhanced ultrasound after intravenous administration of a microbubble contrast agent for differentiation of benign and malignant thyroid nodules: assessment of diagnostic accuracy. Eur Radiol 2012;22:1357-65.
9. Tappouni RR, Itri JN, McQueen TS, Lalwani N, Ou JJ. ACR TI-RADS: Pitfalls, Solutions, and Future Directions. Radiographics 2019;39:2040-52.
10. Liu X, Ouyang D, Li H, Zhang R, Lv Y, Yang A, Xie C. Papillary thyroid cancer: dual-energy spectral CT quantitative parameters for preoperative diagnosis of metastasis to the cervical lymph nodes. Radiology 2015;275:167-76.
11. de Koster EJ, de Geus-Oei LF, Brouwers AH, van Dam EWCM, Dijkhorst-Oei LT, van Engen-van Grunsven ACH, van den Hout WB, Klooker TK, Netea-Maier RT, Snel M, Oyen WJG, Vriens D; EfFECTS trial study group. [18F]FDG-PET/CT to prevent futile surgery in indeterminate thyroid nodules: a blinded, randomised controlled multicentre trial. Eur J Nucl Med Mol Imaging 2022;49:1970-84.
12. Ciappuccini R, Licaj I, Lasne-Cardon A, Babin E, de Raucourt D, Blanchard D, Bastit V, Saguet-Rysanek V, Lequesne J, Peyronnet D, Grellard JM, Clarisse B, Bardet S. (18)F-Fluorocholine Positron Emission Tomography/Computed Tomography is a Highly Sensitive but Poorly Specific Tool for Identifying Malignancy in Thyroid Nodules with Indeterminate Cytology: The Chocolate Study. Thyroid 2021;31:800-9.
13. Merten MM, Castro MR, Zhang J, Durski J, Ryder M. Examining the Role of Preoperative Positron Emission Tomography/Computerized Tomography in Combination with Ultrasonography in Discriminating Benign from Malignant Cytologically Indeterminate Thyroid Nodules. Thyroid 2017;27:95-102.
14. Hamid S, Nasir MU, So A, Andrews G, Nicolaou S, Qamar SR. Clinical Applications of Dual-Energy CT. Korean J Radiol 2021;22:970-82.
15. McCollough CH, Leng S, Yu L, Fletcher JG. Dual- and Multi-Energy CT: Principles, Technical Approaches, and Clinical Applications. Radiology 2015;276:637-53.
16. Lee DH, Lee YH, Seo HS, Lee KY, Suh SI, Ryoo I, You SH, Kim B, Yang KS. Dual-energy CT iodine quantification for characterizing focal thyroid lesions. Head Neck 2019;41:1024-31.
17. Xu XQ, Zhou Y, Su GY, Tao XW, Ge YQ, Si Y, Shen MP, Wu FY. Iodine Maps from Dual-Energy CT to Predict Extrathyroidal Extension and Recurrence in Papillary Thyroid Cancer Based on a Radiomics Approach. AJNR Am J Neuroradiol 2022;43:748-55.
18. Zou Y, Sun S, Liu Q, Liu J, Shi Y, Sun F, Gong Y, Lu X, Zhang X, Xia S. A new prediction model for lateral cervical lymph node metastasis in patients with papillary thyroid carcinoma: Based on dual-energy CT. Eur J Radiol 2021;145:110060.
19. Pearce EN, Farwell AP, Braverman LE. Thyroiditis. N Engl J Med 2003;348:2646-55.
20. Zhang F, Qiao Y, Zhang H. Value of CT Features in the Diagnosis of Papillary Thyroid Tumors in Incidental Thyroid Nodules. Int J Endocrinol 2020;2020:9342317.
21. Song Z, Li Q, Zhang D, Li X, Yu J, Liu Q, Li Z, Huang J, Zhang X, Tang Z. Nomogram based on spectral CT quantitative parameters and typical radiological features for distinguishing benign from malignant thyroid micronodules. Cancer Imaging 2023;23:13.
22. Radzina M, Ratniece M, Putrins DS, Saule L, Cantisani V. Performance of Contrast-Enhanced Ultrasound in Thyroid Nodules: Review of Current State and Future Perspectives. Cancers (Basel) 2021.
23. Li X, Gao F, Li F, Han XX, Shao SH, Yao MH, Li CX, Zheng J, Wu R, Du LF. Qualitative analysis of contrast-enhanced ultrasound in the diagnosis of small, TR3-5 benign and malignant thyroid nodules measuring ≤1 cm. Br J Radiol 2020;93:20190923.

24. Li Q, Song Z, Zhang D, Li X, Liu Q, Yu J, Wen Y, Zhang J, Ren X, Li Z, Zhang X, Tang Z. Diagnostic accuracy of dual-energy computed tomography-based nomogram for differentiating papillary thyroid microcarcinomas from micronodular goiters. Quant Imaging Med Surg 2023;13:3428-40.
25. Kim DW, Jung SJ, Baek HJ. Computed tomography features of benign and malignant solid thyroid nodules. Acta Radiol 2015;56:1196-202.
26. Li HW, Wu XW, Liu B, Liu WD, Gao N. Clinical values of of gemstone spectral CT in diagnosing thyroid disease. J Xray Sci Technol 2015;23:45-56.
27. Cappelli C, Castellano M, Pirola I, Gandossi E, De Martino E, Cumetti D, Agosti B, Rosei EA. Thyroid nodule shape suggests malignancy. Eur J Endocrinol 2006;155:27-31.
28. Wu YY, Wei C, Wang CB, Li NY, Zhang P, Dong JN. Preoperative Prediction of Cervical Nodal Metastasis in Papillary Thyroid Carcinoma: Value of Quantitative Dual-Energy CT Parameters and Qualitative Morphologic Features. AJR Am J Roentgenol 2021;216:1335-43.
29. Kogai T, Hershman JM, Motomura K, Endo T, Onaya T, Brent GA. Differential regulation of the human sodium/iodide symporter gene promoter in papillary thyroid carcinoma cell lines and normal thyroid cells. Endocrinology 2001;142:3369-79.
30. Liou MJ, Lin JD, Chan EC, Liu FH, Chao TC, Weng HF. Detection of mRNA of sodium iodide symporter in benign and malignant human thyroid tissues. Cancer Lett 2000;160:75-80.
31. Luo YH, Mei XL, Liu QR, Jiang B, Zhang S, Zhang K, Wu X, Luo YM, Li YJ. Diagnosing cervical lymph node metastasis in oral squamous cell carcinoma based on third-generation dual-source, dual-energy computed tomography. Eur Radiol 2023;33:162-71.
32. He C, Liu J, Li Y, Lin L, Qing H, Guo L, Hu S, Zhou P. Quantitative parameters of enhanced dual-energy computed tomography for differentiating lung cancers from benign lesions in solid pulmonary nodules. Front Oncol 2022;12:1027985.
33. Chen W, Lin G, Cheng F, Kong C, Li X, Zhong Y, Hu Y, Su Y, Weng Q, Chen M, Xia S, Lu C, Xu M, Ji J. Development and Validation of a Dual-Energy CT-Based Model for Predicting the Number of Central Lymph Node Metastases in Clinically Node-Negative Papillary Thyroid Carcinoma. Acad Radiol 2024;31:142-56.
34. Freedman AN, Seminara D, Gail MH, Hartge P, Colditz GA, Ballard-Barbash R, Pfeiffer RM. Cancer risk prediction models: a workshop on development, evaluation, and application. J Natl Cancer Inst 2005;97:715-23.

Cite this article as: Ren X, Song Z, Zhang D, Li X, Huang J, Liu Q, Wen Y, Zhang J, Zeng D, Tang Z. Differentiation of benign and malignant lesions in Bethesda III and IV thyroid nodules via dual-energy computed tomography quantitative parameters and morphologic features. Quant Imaging Med Surg 2024;14(7):4567-4578. doi: 10.21037/qims-23-1511

